

See discussions, stats, and author profiles for this publication at: <https://www.researchgate.net/publication/270826414>

# Structure-Assisted Functional Anchor Implantation in Robust Metal–Organic Frameworks with Ultralarge Pores

ARTICLE in JOURNAL OF THE AMERICAN CHEMICAL SOCIETY · JANUARY 2015

Impact Factor: 12.11 · DOI: 10.1021/ja5123528 · Source: PubMed

---

CITATIONS

2

READS

120

## 3 AUTHORS:



Jihye Park

Texas A&M University

16 PUBLICATIONS 279 CITATIONS

[SEE PROFILE](#)



Dawei Feng

Texas A&M University

35 PUBLICATIONS 747 CITATIONS

[SEE PROFILE](#)



Hong-Cai Zhou

Texas A&M University

232 PUBLICATIONS 18,785 CITATIONS

[SEE PROFILE](#)

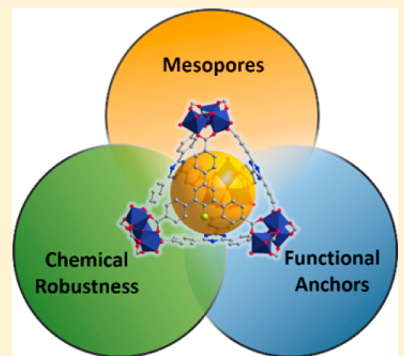
# Structure-Assisted Functional Anchor Implantation in Robust Metal–Organic Frameworks with Ultralarge Pores

Jihye Park, Dawei Feng, and Hong-Cai Zhou\*

Department of Chemistry, Texas A&M University, College Station, Texas 77843-3255, United States

Supporting Information

**ABSTRACT:** A facile functionalization assisted by the structural attributes of PCN-333 has been studied while maintaining the integrity of the parent MOF including ultralarge pores, chemical robustness, and crystallinity. Herein we thoroughly analyzed ligand exchange phenomena in PCN-333 and demonstrate that the extent of exchange can be tailored by varying the exchange conditions as potential applications may require. Through this method a variety of functional groups are incorporated into PCN-333. To further show the capabilities of this system introduction of a BODIPY fluorophore as a secondary functionality was performed to the functionalized framework via a click reaction. We anticipate the PCN-333 with functional anchor can serve as a stable platform for further chemistry to be explored in future applications.



## INTRODUCTION

Ordered mesoporous materials have been extensively studied because of their potential toward practical applications including heterogeneous supports for catalysis, separation, enzyme immobilization, drug delivery, and sensing taking advantage of their high surface areas and large pores.<sup>1</sup> In particular, for large guest molecules such as organometallic species, nanoparticles, and enzymes the mesoporosity is of great importance.<sup>2</sup> Traditional mesoporous materials including mesoporous silica, mesoporous carbon, and metal oxides have paved the ways for such applications, but there are major limitations to these materials such as lack of structural diversity (e.g., pore geometry) and versatile functionality. Moreover, to effectively prevent leaching of the immobilized species, postsynthetic modification of functional groups to covalently anchor the guest species is highly desired. However, it has been challenging due to the lack of easily modifiable sites in these traditional mesoporous materials.<sup>3</sup>

In the last two decades, metal–organic frameworks (MOFs) have emerged as a class of promising organic–inorganic hybrid materials that are composed of metal ions/clusters and bridging organic linkers.<sup>4</sup> Due to their tunable structures derived from a judicious selection of inorganic building blocks and the molecular-level design of organic linkers, MOFs can provide tailor-made structures for desired applications compared with conventional mesoporous materials.<sup>5</sup> Apart from the structural diversity of MOFs, their three-dimensional (3D) cavities can facilitate the accessibility of the guest molecules. Therefore, mesoporous MOFs with predesigned covalent anchors (pendant functional groups) can serve as ideal platforms to immobilize functional species.

However, most MOF materials reported to date are mainly restricted to a microporous regime.<sup>6</sup> Even for mesoporous

MOFs, the accommodation of large molecules into the pores such as bulky catalysts or enzymes is challenging because such large entities will take up a substantial volume of the pore.<sup>7</sup> As a result, efficient diffusion is slowed, and the accessibility of incoming species will be reduced substantially. In addition, introduction of covalent anchors could further reduce the original pore size, leaving even less space to immobilize large species. Most importantly, an excellent stability of the framework is a prerequisite to guarantee the framework intactness, especially with inclusion of immobilized guests working in harsh conditions. However, most reported mesoporous MOFs show relatively weak chemical stability.<sup>8</sup> Therefore, stable MOFs with ultralarge pores and functional groups are highly desired.

Herein we report a facile route to functionalize PCN-333(M) (M = Fe and Sc), a robust MOF isoreticular to MIL-100 with ultralarge pores ( $\sim 5.5$  nm), via postsynthetic ligand exchange that is assisted by structural integrity of PCN-333. A wide range of functional groups were introduced into the PCN-333(M) while maintaining the porosity and crystallinity of the parent framework. Furthermore, several experiments were performed to illustrate a better understanding of the ligand exchange process in PCN-333(Fe). Ultimately, introduction of a secondary functional group into functionalized PCN-333 was successfully demonstrated through click chemistry. These findings will allow for functionalized PCN-333(M) to be used as a useful scaffold for a variety of promising applications by taking advantage of facile functionalization, framework robustness, and ultralarge pores which allow for more possible chemistry within the MOF.

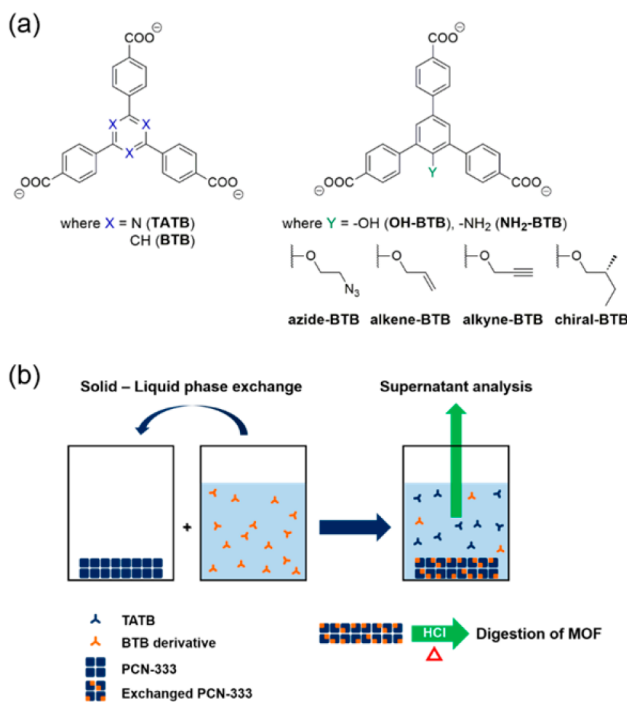
Received: December 3, 2014

## ■ RESULTS AND DISCUSSION

**1. Direct Synthesis of Isoreticular Structure of Functionalized PCN-333(Fe).** Most recently, our group reported a mesoporous MOF, PCN-333, which consists of a trimeric metal cluster and tritopic linker, 4,4',4''-s-triazine-2,4,6-triyl-tribenzoic acid (TATB).<sup>9</sup> PCN-333 ( $M_3O(OH)(TATB)_2$ ) ( $M = Fe, Al, Sc$ ) exhibits the largest cage of 5.5 nm among all reported MOFs. Meanwhile, the trivalent metal nodes endow PCN-333 with excellent chemical stability allowing for its utilization under harsh conditions. Therefore, decoration of PCN-333 with covalent anchors would provide a great platform to immobilize versatile functional species, especially those in the nanoscale, which cannot be successfully accomplished by other MOFs.

Having examined the PCN-333 structure, we chose 1,3,5-benzenetribenzoic acid (BTB) to exchange TATB due to the structural resemblance including molecular size and connectivity. As a result of the 2-position on the central benzene ring of BTB allowing for chemical derivatization (Scheme 1a),

**Scheme 1. (a)** Library of Ligands Involved in Exchange in PCN-333 and (b) Schematic Illustration of Solid–Liquid Phase Ligand Exchange



the functionalized BTB derivative was expected to introduce various covalent anchors into the mesoporous PCN-333. A series of ligands bearing different functional groups were synthesized. The covalent anchor was designed to occupy only a small portion of the pores while leaving most space available for the immobilization of large guest species. Therefore, we intuitively attempted a direct synthesis of functionalized PCN-333 from preinstalled functional groups on the BTB derivatives. Direct synthesis was performed by using the kinetically tuned dimensional augmentation (KTDA) method with preformed cluster  $Fe_3(O)(CH_3COO)_6$  as a starting material to obtain isoreticular structures of PCN-333 with BTB and OH-BTB.<sup>10</sup> Although large single crystals of Fe-MOFs, PCN-260, and PCN-262 were harvested, respectively, single crystal X-ray

diffraction revealed different structures even in the presence of the same inorganic building block,  $Fe_3(O)(COO)_6$ , as in PCN-333 (Figure 1b).

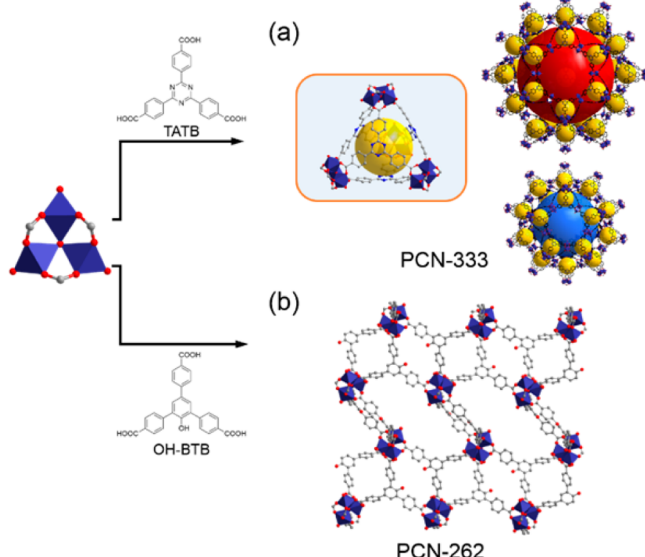


**Figure 1.** (a) Structure of PCN-333 with three different cages. (b) Structure of PCN-262, a direct synthesis product from OH-BTB.

As shown in Figure 2a, the structure of PCN-333 is built from a supertetrahedron unit, of which each face is a TATB

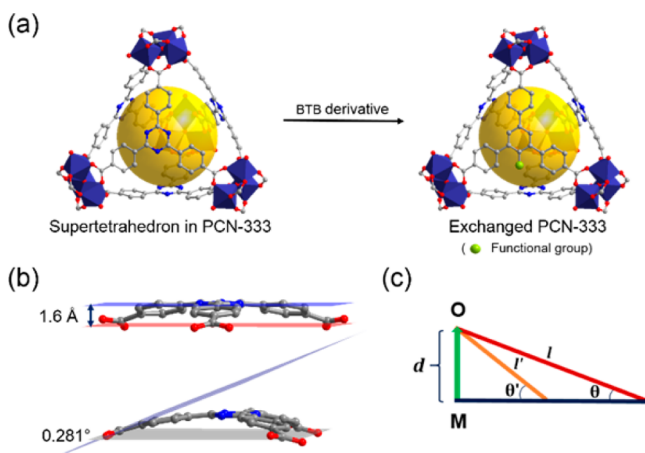


**Figure 2.** (a) Scheme of ligand exchange in supertetrahedron in PCN-333. (b) One face of supertetrahedron in PCN-333 showing the distance (top) and the angle (bottom) in the bent geometry. (c) Schematic illustration of M–O dissociation.

linker. Although TATB does not adopt perfect  $D_{3h}$  symmetry in the framework, six oxygen atoms on TATB reside in the same plane which gives rise to a stable tetrahedral cage in  $C_{3v}$  symmetry from bent geometry (Figure 2b). However, coplanar  $D_{3h}$  symmetry of BTB is highly energetically unfavored due to the repulsion between H atoms on the central benzene ring and the three peripheral benzene rings. With BTB derivatives, the attached functional groups on the central benzene ring would cause additional steric hindrance resulting in even higher energy of the coplanar geometry. Considering *in situ* MOF synthesis, when possible inorganic nodes have a negligible energy difference, a major product is dominated by energy

demands of linkers. Because free rotation of single bonds in the BTB derivative allows the linker to stay in a lower energy conformation in solution, TATB and BTB derivatives could lead to different structures with the same inorganic node,  $\text{Fe}_3(\text{O})$ , where preferential conformation of linkers dominates the final products. Although the isostructure of PCN-333 constructed with BTB has been reported,<sup>6n</sup> the functionalized isoreticular structure of PCN-333 cannot be achieved through the direct synthetic approach.

**2. Structure-Assisted Ligand Exchange Process.** Due to ligand conformation dominating the framework growth process in direct synthesis leading to an unwanted structure, we turned to the postsynthetic ligand exchange method.<sup>11</sup> Postsynthetic ligand exchange (PSE) and solvent-assisted linker exchange (SALE) have appeared as powerful routes to modify a parent MOF in which the ligand exchange occurs in relatively stable MOFs with a functionalized incoming ligand. For instance, Cohen and co-workers studied ligand exchange in UiO-66(Zr), and several MIL series with bromo and amino analogues of the original ligands.<sup>11f,g,i</sup> The Hupp group also demonstrated solvent-assisted linker exchange in a ZIF series.<sup>11d,e</sup> Also, using stepwise ligand exchange strategy, establishment of extended isoreticular structures has been studied.<sup>11b,m,o</sup> To establish a versatile platform having large pores and chemical stability via postsynthetic ligand exchange in PCN-333(Fe), we started from BTB, the simplest form bearing a resemblance to TATB, as the exchanging ligand. With thoroughly washed PCN-333(Fe), ligand exchange was performed via a biphasic (solid–liquid) manner as illustrated in Scheme 1b. To exclude a dissolution–recrystallization pathway, the exchange reaction was performed under lower temperature than that of the MOF synthetic condition.<sup>9</sup>

Despite many noticeable examples that have shown postsynthetic ligand exchange in stable MOFs, there has not yet been a successful example demonstrating ligand exchange in extremely stable mesoporous MOFs, such as MIL-100 and MIL-101, although both MOFs have been widely employed in many applications. Surprisingly, a successful ligand exchange was achieved in PCN-333(Fe) by using BTB as the incoming ligand. In general, most ligand substitution reactions in octahedral complexes undergo a dissociative pathway. The rate-determining step in the dissociative pathway is known to be a breaking of metal–ligand (M–L) bond.<sup>12</sup> Similarly, the ligand exchange process in MOF can be generalized to the principle in coordination chemistry that the M–L bond should be dissociated to exchange ligands. MIL-101 and MIL-100 have been reported as extremely robust frameworks, suggesting strong coordination (M–L bond) in these two MOFs which in turn leads to an extremely slow bond dissociation rate for the ligand exchange. One reason that could account for this is the strong electrostatic interaction between carboxylates and the high  $Z/r$  valued trivalent metal ions used in these MOFs. To achieve an effective ligand exchange, therefore, longer reaction time and/or higher temperature might be expected in these frameworks.

However, the exchanging environment provides not only extra carboxylates (from incoming ligands) but also solvent molecules as competing reagents, both of which could destruct the framework by forming fractions or amorphous products. Therefore, in the extremely robust MIL-101 and MIL-100, the frameworks could be severely damaged before an apparent exchange happens. On the contrary, PCN-333(Fe), an isoreticular structure of MIL-100, showed successful ligand

exchange. As the bond nature is identical in both frameworks, the elongation of the linker could explain the exchange event. Unlike common coordination complexes, each linker in MOFs binds to multiple metal nodes. Considering that a complete ligand exchange of a linker includes breaking of all coordinated carboxylates, the case where only one of them is dissociated while the others remain bound onto the framework prevents total dissociation. Consequently, the structural restraint from multiple coordination sites impedes complete ligand dissociation, which eventually slows the ligand exchange in the framework. In addition, when the connectivity of the linker is higher, it takes more steps for the complete ligand dissociation, resulting in a more difficult exchange process. Furthermore, for similar linkers of differing length, the extent of such restraint varies. For instance, assuming  $d$  in Figure 2b (describing only one binding site) stands for a distance allowing for efficient dissociation–association of the ligand exchange. When the dissociation is happening (moving distance to  $d$ ), longer linker  $l$  takes a smaller angle  $\theta$  compared to that of shorter linker  $l'$ , which would result in less strain to the remaining coordination sites on the linker. If  $l$  gets infinitely longer, then the structural restraint from each coordination site becomes negligible, and the dissociation process in the MOF would be similar to the case of a small coordination complex in a homogeneous system. Therefore, ligand exchange can happen more easily in isoreticular structures constructed with longer linkers.

In the supertetrahedron of PCN-333,  $\text{Fe}_3(\text{O})$  clusters act as vertexes. The dihedral angle between the carboxylate plane and the  $\text{Fe}_3(\text{O})$  plane is inherently determined by the octahedral coordination environment of each Fe atom. However, it is not precisely compatible to be directly connected in the triangular face of a perfect tetrahedron ( $0.281^\circ$ ) as shown in Figure 2b. Thus, TATB must adopt a bent geometry to hold three  $\text{Fe}_3(\text{O})$  clusters in the supertetrahedron unit. This generates a distance of about 1.6 Å between the center of TATB and the ideal triangular plane formed by six oxygen atoms in the tetrahedron, which suggests TATB would bear high energy (Figure 2b). Although bond dissociation happens between the carboxylate and Fe, such an energetically unfavorable conformation would still facilitate the dissociation in order to lower the energy of the linker. In the meantime, TATB is almost twice as large as benzene-1,3,5-tricarboxylic acid (BTC), which makes all cages in PCN-333 much larger than that in MIL-100, and thereby such extra space allows for faster diffusion of both incoming and dissociating ligands to further promote the ligand exchange process in PCN-333. All structural features of PCN-333 including the greatly bent conformation of TATB, less mutual restriction between each coordinating site because of its larger size (compared to MIL-100), and extremely large pores assist the ligand exchange in spite of the strong M–L bond, all combined make this system the first example of successful ligand exchange in highly robust mesoporous MOF with tritopic linkers.

**3. Optimization of Ligand Exchange in PCN-333(Fe) with BTB.** Systematic studies to further investigate the ligand exchange process in PCN-333(Fe) were performed. First, PCN-333(Fe) was incubated for 24 h in BTB stock solution at different temperatures [room temperature (rt), 85 °C, 100 °C]. Upon completion of ligand exchange, the relative composition of the ligands (BTB was used excess amount) was analyzed by <sup>1</sup>H NMR of the resulting supernatant. The ligand exchange reaction at room temperature showed the lowest content of TATB (~1%) while both higher temperatures (85 °C, 100 °C)

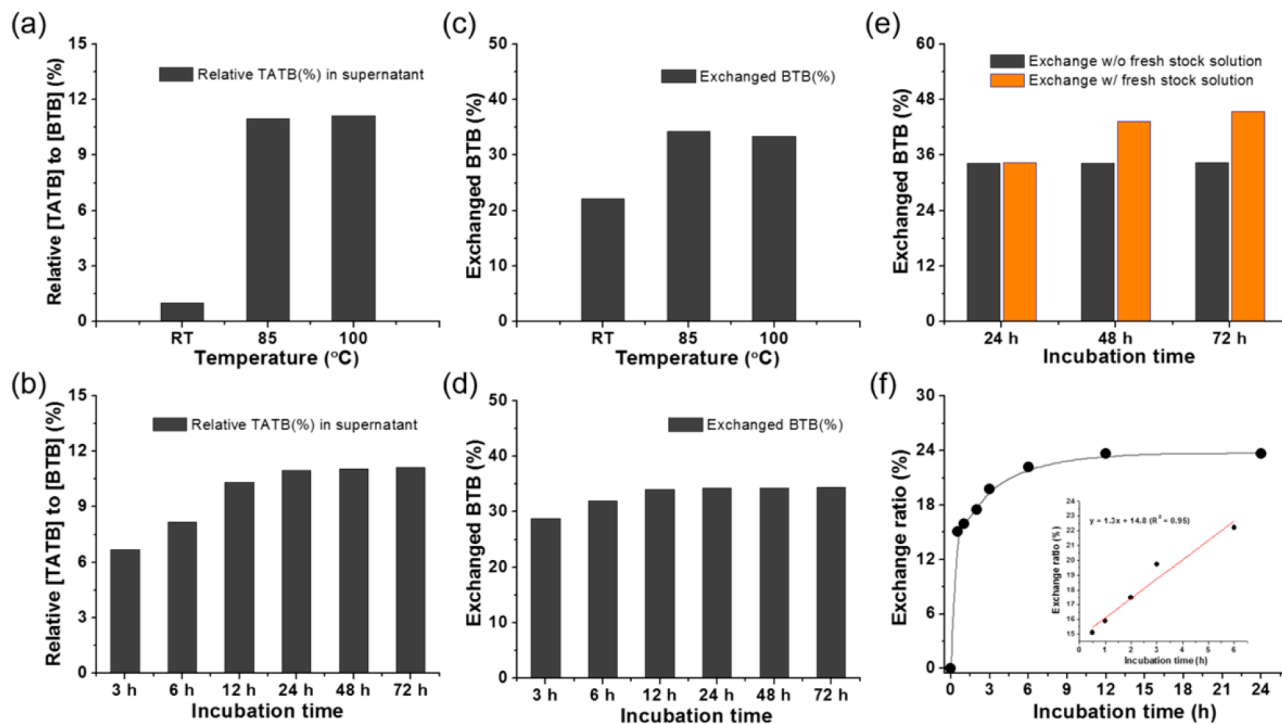


**Figure 3.** (a) Relative TATB (%) in supernatant at different temperatures (incubation time = 24 h). (b) Time-dependent relative TATB (%) in supernatant (incubation temperature = 85 °C). (c) Ratio of exchanged BTB (%) in PCN-333(Fe) incubated at different temperatures (incubation time = 24 h). (d) Ratio of exchanged BTB (%) in PCN-333(Fe) at different incubation times (incubation temperature = 85 °C). (e) Comparison of BTB exchange ratio (%) in PCN-333(Fe) upon provision of fresh stock solution. (f) BTB exchange ratio (%) in PCN-333(Sc) as a function of incubation time.

yielded higher contents of TATB (~11% for both) coming out from the parent MOF, which indicates the ligand exchange was facilitated at higher temperatures (Figure 3a). Next, the ligand exchange process was investigated for different incubation times. The supernatants of BTB exchanged PCN-333(Fe) samples were taken after different incubation times at 85 °C. The <sup>1</sup>H NMR spectroscopy showed the supernatant incubated for 3 h was composed of ~7% of TATB relative to BTB and the ratios of TATB gradually increased as incubation time increased up to 24 h. However, the exchange ratios were saturated at a longer period of exchange process (72 h), and almost the same concentrations of TATB were obtained (~11%) (Figure 3b).

As supernatant analyses merely indicate the exchange event indirectly, <sup>1</sup>H NMR spectroscopy of digested MOFs was performed to determine the absolute composition of exchanged PCN-333(Fe). Due to the high chemical stability of exchanged PCN-333(Fe), the samples were treated with concentrated HCl (37%) and refluxed for 12 h to be digested. The digested sample that was incubated at room temperature showed 22% exchange of BTB. Consistent with the previous observations from the supernatant, the samples exchanged at 85 and 100 °C showed higher extent of exchange, 34% and 33%, respectively (Figure 3c). The effect of incubation time was also examined on the digested samples. The exchange ratios gradually increased from 29% (3 h exchanged sample) to ~34% (12–72 h exchanged samples) (Figure 3d). Similar to the results from supernatant studies, the composition of BTB did not increase with extension of incubation time longer than 24 h. Ligand exchange in PCN-333(Fe) showed a faster rate of exchange in that approximately 30% exchange could be achieved within 3 h under mild conditions. Also, these findings clearly showed promise that the degree of exchange can be

modulated by controlling temperature and exchange time. Powder X-ray diffraction of these samples indicates that the structural integrity of parent PCN-333(Fe) was well-retained after the ligand exchange (Figure 5a).

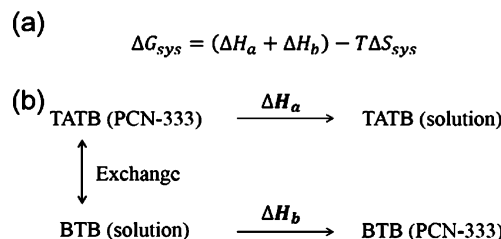


**Figure 4.** (a) Gibbs free energy change of the system for ligand exchange in PCN-333. (b) Enthalpy change of the system during ligand exchange.

After discovering the previous result, we further sought to find whether the exchange ratio could become higher or whether there would be a maximum extent of exchange within a capacity allowing the retention of framework. To drive the equilibrium of the system forward, the supernatant was exchanged with fresh BTB stock solution every 24 h. Ligand exchange was performed by following the routine procedure at 85 °C. A higher BTB exchange ratio (~45%) was achieved when the fresh stock solution was provided after 24 h during 48 h of exchange. However, there was no significant increase when fresh BTB solution was subsequently provided each day for longer periods of time (Figure 3e).

**4. Thermodynamics behind Ligand Exchange in PCN-333.** Having observed that the exchange ratio stopped

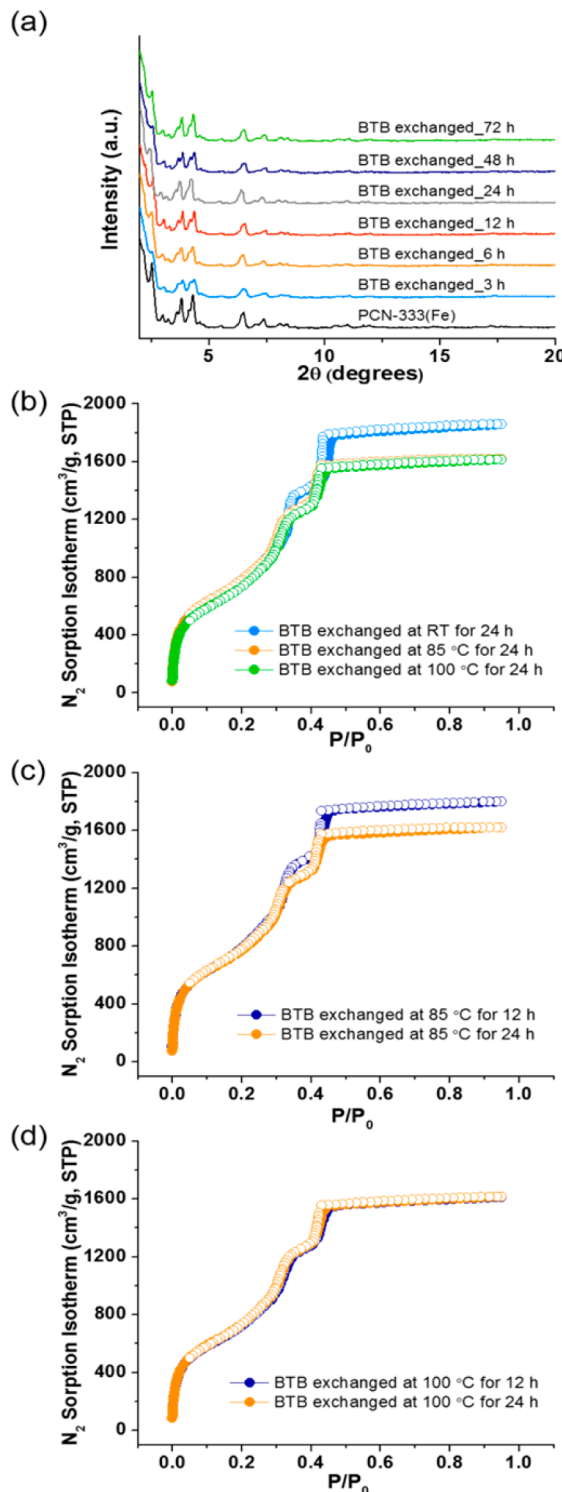


**Figure 5.** (a) PXRD patterns of BTB exchanged PCN-333(Fe) for different incubation times. Ligand exchange was performed at 85 °C. (b) N<sub>2</sub> sorption isotherms of BTB-exchanged PCN-333(Fe) performed at different temperatures. (c) N<sub>2</sub> sorption isotherms of BTB-exchanged PCN-333(Fe) for different incubation times at 85 °C. (d) N<sub>2</sub> sorption isotherms of BTB exchanged PCN-333(Fe) for different incubation times at 100 °C.

increasing after a certain point despite successive provision of fresh incoming ligands while maintaining crystallinity of PCN-333(Fe), we further sought to understand the process in our

system (see section 11 in Supporting Information for detailed rationales of ligand exchange in PCN-333).

At the very beginning of the ligand exchange process, the drastic entropy increase ( $\Delta S_{sys}$ ) results in a negative  $\Delta G_{sys}$ , which spontaneously drives the exchange reaction forward. When the concentration of TATB in solution increases up to a certain point,  $\Delta S_{sys}$  would be insufficient to maintain the negative value of  $\Delta G_{sys}$ , and eventually, an equilibrium is established where  $\Delta G_{sys} = 0$ . Such rationale is consistent with the experimental results that the maximum exchange ratio was observed for each batch of BTB exchanged sample.

Thus, the exchange of fresh BTB stock solution reinitiated the high entropy increasing process. To some extent, a new equilibrium was established, but over time the exchange ceased again. Ideally, the ligand exchange process could keep going close to full exchange (~100%) upon successive provision of fresh incoming ligands. In the case of PCN-333, however, the exchange process was terminated when the system reached a certain exchange ratio regardless of whether refilling of fresh BTB solution occurred (Figure 3e). This may imply the total enthalpy change ( $\Delta H_a + \Delta H_b$ ) is no longer the same value as in the circumstance of low BTB exchange ratio in PCN-333. In other words,  $\Delta H_b$  becomes an even larger positive value whereas  $\Delta H_a$  remains the same, which leaves the framework in high energy when more BTB molecules are inserted after the maximum tolerance that PCN-333 can bear until its destruction. As a result, the ligand exchange can hardly be driven further by the entropy change ( $\Delta S_{sys}$ ) due to the huge enthalpy increase ( $\Delta H_a + \Delta H_b$ ) and the saturation point appears. Theoretically, raising the temperature (increasing  $T\Delta S_{sys}$  value) could overcome such enthalpy increase ( $\Delta H_a + \Delta H_b$ ) to further drive the ligand exchange process.

However, the increased temperature could also destroy the framework as previously discussed. Thus, a balance must be struck by controlling temperature to affect optimum ligand exchange process while maintaining framework integrity.

To examine whether an *exchange saturation point* (maximum exchange ratio) lies on the thermodynamic equilibrium, we further carried out a reverse ligand exchange reaction using extra TATB to replace the inserted BTB in the exchanged PCN-333. When TATB from the solution replaces the inserted BTB in the framework, the enthalpy change will be inverted to a negative value,  $-(\Delta H_a + \Delta H_b)$ . Because the entropy change maintains a similar trend (a positive value), the overall change in Gibbs free energy will become negative to spontaneously drive the exchange process (reverse reaction). As expected, after soaking BTB-exchanged PCN-333(Fe) into TATB solution for 12 h at 85 °C, the composition of BTB in the reversibly exchanged PCN-333(Fe) decreased from ~35% to less than 6% with well-retained crystallinity, validating the explanation for the presence of the *exchange saturation point* in the system (see section 9 in Supporting Information).

As previously discussed, framework destruction is inevitable during the ligand exchange process due to the competing association–dissociation at the M–L bond from extra ligands in the solution and some solvent dissociates such as formate. When the exchange is extremely slow, the framework can be destroyed before evident exchange happens, which would result in unsuccessful exchange as in the case of MIL-101 and MIL-100. In order for successful ligand exchange in the robust MOF, optimization becomes important to balance the exchange ratio and framework intactness. To optimize such a balance of the exchange ratio, porosity and crystallinity of exchanged PCN-

333(Fe), the nitrogen sorption measurement and PXRD were employed. As shown in Figure 5b, when the exchange reaction was conducted for 24 h at different temperatures, the lower temperature (rt) gave the better porosity than that of higher temperatures (85 °C, 100 °C). Although a slight decrease in porosity (~13%; relative to the parent MOF) was observed for the samples treated at higher temperatures, they still exhibited high porosity. We then examined whether the incubation time affects the porosity as well. For the exchanged PCN-333(Fe) incubated at 85 °C, shorter reaction time (12 h) rendered better porosity than that of longer exchange time (24 h) (Figure 5c).

### 5. Ligand Exchange with Various Functional Groups.

One of the most valuable advantages of MOFs over other conventional porous materials is synthetic versatility from the design of diverse ligands. Utilizing the powerful tool of organic chemistry, we sought to expand our library of ligands to accommodate various functional groups in PCN-333(Fe) through the structure-assisted ligand exchange process. Most incoming BTB derivatives with various substituents at the 2-position of the central benzene ring (Scheme 1a) were synthesized from OH-BTB via a simple nucleophilic substitution reaction with excellent quantitative yields (Supporting Information, section 2).

Ligand exchange of BTB derivatives in PCN-333(Fe) was performed by adopting the optimized condition from BTB exchange studies (85 °C, 12 h). A 12 h period of incubation time was chosen as a shorter reaction time and gave better porosity with compatible extent of exchange. Photographs of the exchanged samples are shown in Figure 6a. Notably, distinctive color changes were observed for the samples exchanged with OH-BTB (olive) and NH<sub>2</sub>-BTB (dark brown), which clearly indicate the incorporation of different ligands. To determine the exchange ratio for each ligand, <sup>1</sup>H NMR spectra of the digested samples were taken. The exchange ratio for each ligand is summarized in Table 1. Presumably due to different enthalpy changes ( $\Delta H_b$ ) of each ligand before and after ligand exchange resulting from their different solubility as well as steric and/or electronic effects, each ligand showed different extent of exchange ranging from 18.0% to 39.4% under identical conditions. Nevertheless, all of the functionalized BTB ligands were successfully exchanged into PCN-333(Fe) with significant exchange ratios. Figure 6b shows well-maintained crystallinity of exchanged samples regardless of the functional groups (Figure 6b). Particularly, infrared (IR) spectroscopy of the azide-BTB exchanged PCN-333(Fe) shows a characteristic stretching band at 2106 cm<sup>-1</sup>, which is indicative of the presence of an azide group (Supporting Information, section 6, Figure S22). The porosity of each exchanged PCN-333(Fe) sample was then evaluated by N<sub>2</sub> adsorption measurements at 77 K. As expected, the total uptake of each sample slightly decreased after the exchange with a functionalized ligand (Figure 6c). However, it is worth noting that the decrease in total pore volume of exchanged PCN-333(Fe) compared to that of the parent material was not critical (approximately decreasing in a range from 7% to 18%, Table 1). To the best of our knowledge, our materials exhibit one of the highest N<sub>2</sub> uptakes among all reported mesoporous MOFs with functionalized covalent anchors.<sup>110,8d</sup> Slight shifts to the lower pressures in steps of the N<sub>2</sub> adsorption isotherm, in comparison to that of the parent material at approximately 0.32 P/P<sub>0</sub> and 0.44 P/P<sub>0</sub>, were observed suggesting changes in pore size due to the incorporation of ligands with substituents.

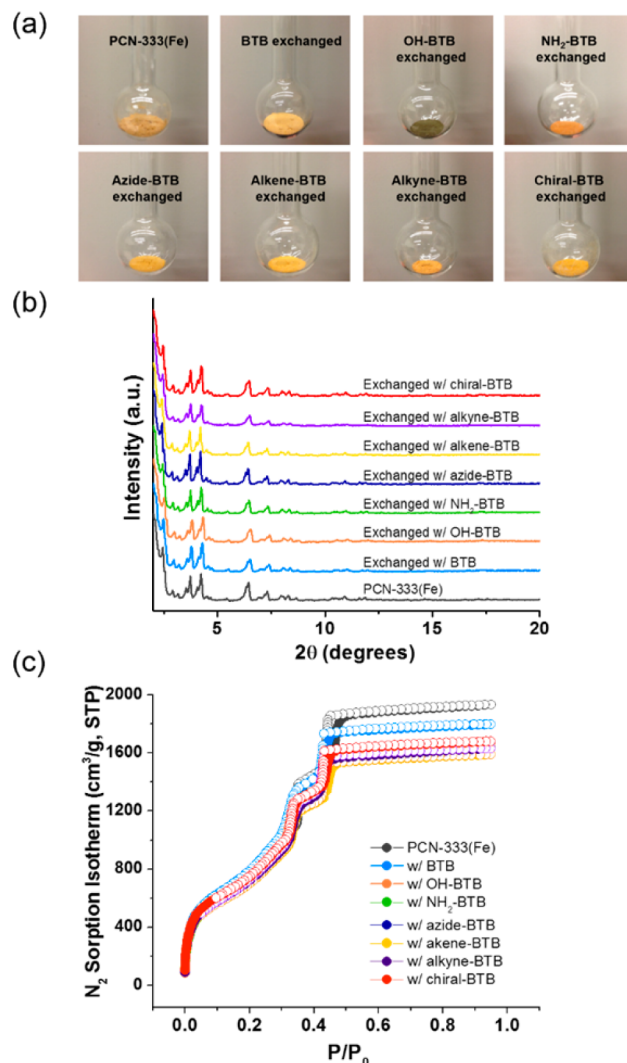


**Figure 6.** (a) Photographs of PCN-333(Fe) samples after ligand exchange with different BTB derivatives (after activation). (b) PXRD patterns of exchanged PCN-333(Fe) with different BTB derivatives. (c) Nitrogen sorption isotherms of PCN-333(Fe) exchanged with different BTB derivatives. Incubation temperature = 85 °C. Incubation time = 12 h.

**Table 1. Summary of N<sub>2</sub> Sorption Isotherm Measurement**

ligand <sup>a</sup>	exchange ratio <sup>b</sup> (%)	N <sub>2</sub> uptake <sup>c</sup> (cm <sup>3</sup> /g, STP)	BET surface area (m <sup>2</sup> /g)
BTB	35.0	1797	3903
OH-BTB	27.5	1657	3595
NH <sub>2</sub> -BTB	18.0	1632	3448
azide-BTB	31.0	1676	3559
alkene-BTB	26.5	1587	3391
alkyne-BTB	39.4	1631	3463
chiral-BTB	27.3	1679	3624

<sup>a</sup>Structures are given in Scheme 1a. <sup>b</sup>Ligand exchange was performed at 85 °C for 12 h. <sup>c</sup>N<sub>2</sub> sorption was measured at 77 K.

DFT pore size distribution analysis showed that the smallest pore, which corresponds to the supertetrahedron unit, was affected the most by appended functional groups on the BTB derivatives compared to that of parent MOF (see Supporting

Information section 5). For example, the pore size distribution of the PCN-333(Fe) exchanged with azide-, alkene-, alkyne-, and chiral-BTB that contains larger functional groups showed a sharper shift in distribution toward the smaller pores than that of BTB, OH-BTB, or NH<sub>2</sub>-BTB exchanged PCN-333(Fe). In comparison, the middle-sized cages and the largest cages are less affected. Assuming the inserted BTB derivatives are well-distributed, the exchange extent exceeding 25% would suggest at least one face of the supertetrahedron is replaced. While the additional functional groups reduce the available space inside of the smallest cage, the middle-sized and especially the largest cages are much less affected due to their inherent ultralarge pores. Therefore, characteristics of mesoporous PCN-333 should be mostly preserved after the implantation of the functional anchors.

**6. Introduction of Secondary Functionality.** After successful implantation of covalent anchors into PCN-333, further examinations were performed on azide-functionalized PCN-333(M) (M = Fe, Sc) to demonstrate introduction of secondary functionality via click chemistry.<sup>8d,11c,13</sup> As previously found, before reaching the exchange saturation point providing fresh stock solution of the incoming ligand increased the exchange ratio.

Taking this into account, the characteristic peak of the azide group at 2106 cm<sup>-1</sup> was monitored by infrared spectroscopy upon increasing the azide group ratio. As fresh stock solution was continuously provided, a more prominent azide stretching band at 2106 cm<sup>-1</sup> was observed in the exchanged sample which indicates the incorporation of more azide-BTB ligands in PCN-333(Fe) (Figure 7a). Knowing this, a click reaction

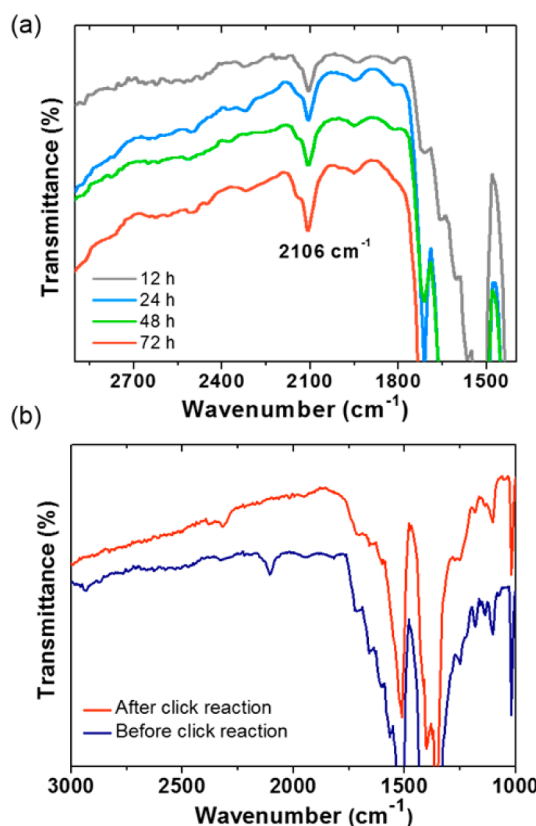


**Figure 7.** (a) IR spectra of azide-BTB exchanged PCN-333(Fe) having different ratios of azide-BTB. (b) Comparison of IR spectra of before/after click reaction with azide-BTB exchanged PCN-333(Fe).

between the azide-functionalized PCN-333(Fe) and methyl propiolate was performed in the presence of CuI in DMF (65 °C, 20 h). The disappearance of this azide IR peak at 2106 cm<sup>-1</sup> shown in Figure 7b suggests a successful anchorage of methyl propiolate as well as completion of the click reaction. The PXRD pattern of the clicked sample also confirmed well-maintained crystallinity owing to the robustness of PCN-333(Fe) (Supporting Information Figure S26).

To investigate the potential utility of functionalized PCN-333, we further sought to expand our experimental design by introducing 4,4-difluoro-4-bora-3a,4a-diaza-s-indaene (BODIPY), a well-known fluorophore due to its excellent photochemical stability, tunable photophysical properties, and high quantum yield. Fluorescence measurements involve high sensitivity and rapid implementation, and thus fluorophores such as BODIPY derivatives can be widely employed in the MOF field. However, the incorporation of fluorophores in MOF as ligands would take substantial synthetic efforts while the anchorage of such compounds to a functionalized MOF through a postsynthetic approach is more practical.<sup>14</sup> To illustrate our concept, terminal alkyne functionalized BODIPY (**14**) was synthesized to perform a click reaction with azide-functionalized PCN-333(Fe). Although the IR spectrum suggests a successful click reaction on PCN-333(Fe), attempts to observe fluorescence from BODIPY-clicked PCN-333(Fe) were not successful due to the presence of Fe(III) which can quench the emission of BODIPY (Supporting Information Figure S28). To avoid the interference from the Fe(III) node, we chose colorless PCN-333(Sc) to show the click reaction more clearly.

The exchanged samples with different ratios of the azide group were prepared by changing the stock solution as previously found. The extent of azide-BTB exchange was determined by <sup>1</sup>H NMR spectroscopy upon digestion of samples (Supporting Information Figure S29). Considering carboxylates bind less strongly to Sc(III) than Fe(III), ligand exchange in PCN-333(Sc) should occur more easily. As observed in the exchanging process, ligand exchange in PCN-333(Sc) reached an equilibrium quickly because of the easier M–L bond dissociation (Figure 3f). However, the thermodynamic equilibrium of the exchange process was almost independent from M–L bond nature as we analyzed and a slightly lower extent of the exchange saturation point was observed in BTB exchange. Nonetheless, azide-functionalized BTB showed a comparable exchanged ratio in PCN-333(Sc) as in PCN-333(Fe) (Supporting Information section 8). The click reaction of azide-functionalized PCN-333(Sc) and alkyne-BODIPY (**14**) was successfully performed with a catalytic amount of CuI in THF (65 °C, 21 h) (Figure 8a). To our delight, BODIPY-clicked PCN-333(Sc) showed strong fluorescence in both suspension and solid-state. Notably, the emission of BODIPY-clicked PCN-333(Sc) in the solid state is green ( $\lambda = 550$  nm; Figure 8b) suggesting that the clicked dye behaves as a monomeric dye, while dye aggregates (**14**) showed a red emission (Figure 8c). After close examination of the structure of PCN-333, it is very likely that the large pores provide enough space for clicked dyes to be spatially separated thereby emitting as single dye molecules. A click reaction on the samples containing different loading of azide groups showed that higher loading of azide groups resulted in a slight red shift in emission maxima (Supporting Information Figures S32 and S33).

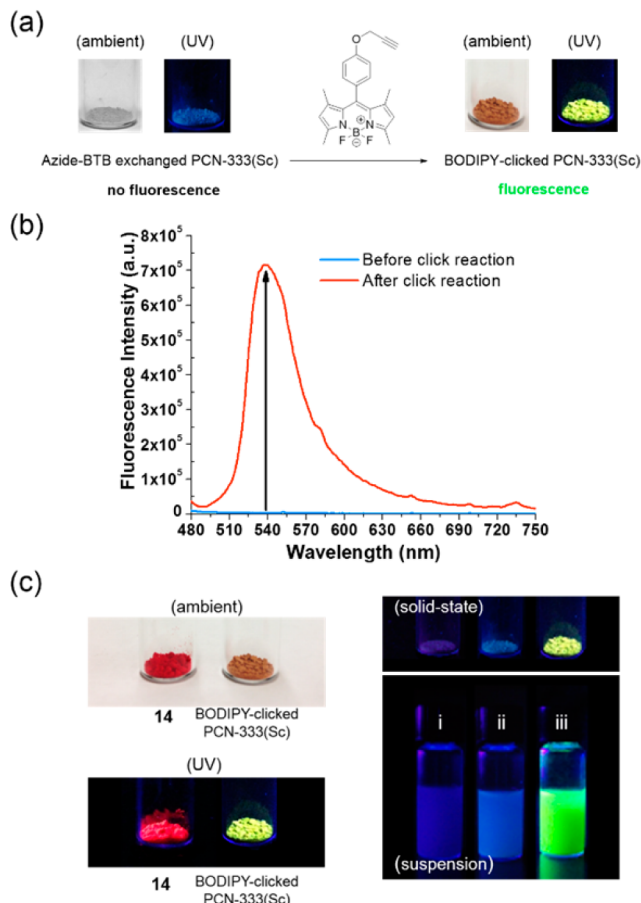


**Figure 8.** (a) Click reaction scheme performed on PCN-333(Sc) with BODIPY fluorophore. Photographs are before and after BODIPY introduction on PCN-333(Sc). (b) Solid-state fluorescence emission spectra of azide-BTB exchanged PCN-333(Sc) (blue) and BODIPY-clicked PCN-333(Sc) (red).  $\lambda_{\text{ex}} = 450 \text{ nm}$ . (c) Comparison of solid-state **14** and BODIPY-clicked PCN-333(Sc) (left). Photographs of (i) pristine PCN-333(Sc), (ii) azide-BTB exchanged PCN-333(Sc), and (iii) BODIPY-clicked sample in both solid-state and suspension (right).

## EXPERIMENTAL SECTION

**Instrumentation.** Nuclear magnetic resonance (NMR) spectra were recorded on Varian Inova 500 spectrometer unless otherwise noted. Powder X-ray diffraction (PXRD) was carried out on a Bruker D8-Focus Bragg–Brentano X-ray powder diffractometer equipped with a Cu sealed tube ( $\lambda = 1.54178$ ) at 40 kV and 40 mA. Thermogravimetric analyses (TGA) were conducted on a Shimadzu TGA-50 thermogravimetric analyzer from 25 to 600 °C at a ramp rate of 2 °C/min in a flowing nitrogen atmosphere. Fourier transform infrared (FT-IR) measurements were performed on a Shimadzu IR Affinity-1 spectrometer. N<sub>2</sub> adsorption–desorption isotherms at 77 K were measured by using a Micrometrics ASAP 2420 system. A high-purity grade (99.999%) of gas was used throughout the sorption experiments. Sample was activated by solvent exchange (in several cycles using fresh acetone), followed by degassing at elevated temperature (150 °C) for 5 h. Details are given in the Supporting Information.

**Direct Synthesis of PCN-260.** BTB (10 mg), FeCl<sub>3</sub>, or Fe<sub>2</sub>CoO(CH<sub>3</sub>COO)<sub>6</sub> (10 mg), and acetic acid (0.25 mL) in 2 mL of NMP were ultrasonically dissolved in a Pyrex vial. The mixture was heated in 150 °C oven for 24 h. After cooling down to room temperature, dark brown crystals were harvested by filtration.

**Direct Synthesis of PCN-262.** OH-BTB (10 mg), FeCl<sub>3</sub> or Fe<sub>2</sub>NiO(CH<sub>3</sub>COO)<sub>6</sub> (10 mg), and acetic acid (0.20 mL) in 2 mL of

DMF were ultrasonically dissolved in a Pyrex vial. The mixture was heated in 150 °C oven for 15 h. After cooling down to room temperature, dark brown crystals were harvested by filtration.

**Synthesis of PCN-333(Fe).** H<sub>3</sub>TATB (60 mg), anhydrous FeCl<sub>3</sub> (60 mg), and trifluoroacetic acid (0.6 mL) were dissolved in 10 mL of DEF. The mixture was heated in 150 °C oven for 12 h until a brown precipitate formed. The resulting brown precipitate was centrifuged and washed with fresh DMF several times.

**Synthesis of PCN-333(Sc).** H<sub>3</sub>TATB (80 mg) and anhydrous ScCl<sub>3</sub>·6H<sub>2</sub>O (200 mg) were dissolved in 10 mL of DMF. The mixture was heated in 150 °C oven for 2 h until a white precipitate formed. The resulting white precipitate was centrifuged and washed with fresh DMF several times.

**General Procedure for Ligand Exchange of PCN-333(Fe).** First, synthesized PCN-333(Fe) (ca. 50 mg) was thoroughly washed with hot DMF, and the isolated sample was then incubated with a stock solution of BTB or BTB derivatives (50–55 mg in DMF) at different temperatures (rt, 85 °C, 100 °C). Upon completion of ligand substitution, the supernatant was removed to examine whether there was TATB that came from the parent MOF after the exchange of ligand. The aliquot of supernatant was filtered through a syringe filter to exclude the possibility of exchanged PCN-333(Fe) crystals remaining, and ligands were recovered by acidification with few drops of 1 M HCl, followed by washing with water. The resulting precipitates were dried and analyzed by <sup>1</sup>H NMR spectroscopy.

**MOF Digestion.** Approximately 15 mg of each ligand exchanged PCN-333(Fe) sample was digested with 37% HCl, refluxed overnight, and washed with water until a neutral pH was reached. DMSO-*d*<sub>6</sub> (0.6 mL) was added to dissolve the ligands. The <sup>1</sup>H NMR spectrum (500 MHz) of exchanged PCN-333(Fe) was collected at room temperature (~21 °C).

**Click Reaction.** Compound **14** (5 mg) was added to a mixture of azide-BTB exchanged PCN-333(Sc) (10 mg) and CuI (0.5 mg) in THF (1.0 mL) in a 4 mL vial. The reaction mixture was stirred at 60 °C for 20 h. The resulting precipitate was collected by centrifugation, washed thoroughly with DMF followed by acetone, and dried to afford a light brown solid in quantitative yield.

## CONCLUSION

In summary, a facile functionalization assisted by structural attributes of PCN-333 has been studied while maintaining the integrity of the parent MOF including ultralarge pores, chemical robustness, and crystallinity. The foregoing results showed a promise that the extent of exchange can be tailored by varying temperature, concentration, or incubation time as potential applications may require. Furthermore, a variety of functional groups can be incorporated into PCN-333 via this strategy to covalently anchor guest species. Along this line, introduction of a secondary functionality was successfully performed via a click reaction with a BODIPY fluorophore. We anticipate the functionalized PCN-333 can serve as a stable platform for further chemistry to be explored in future applications.

## ASSOCIATED CONTENT

### S Supporting Information

Full details for sample preparation and characterization results, and crystallographic data (CIF). This material is available free of charge via the Internet at <http://pubs.acs.org>.

## AUTHOR INFORMATION

### Corresponding Author

zhou@mail.chem.tamu.edu

### Notes

The authors declare no competing financial interest.

## ACKNOWLEDGMENTS

J.P. was supported by ARPA-e of the U.S. Department of Energy through the Methane Opportunities for Vehicular Energy (MOVE) program under the award number DE-AR0000249. D.F. was supported by The Welch Foundation under award number A-1725. H.-C.Z. was supported as part of the Center for Gas Separations Relevant to Clean Energy Technologies, an Energy Frontier Research Center funded by the U.S. Department of Energy, Office of Science, and Office of Basic Energy Sciences under award number DE-SC0001015, and also partially funded by DE-AR0000249. We thank Mr. Kecheng Wang, Ms. Mary Layne Harrell, and Mr. Zachary Perry for helpful discussion.

## REFERENCES

- (1) (a) Vallet-Regí, M.; Balas, F.; Arcos, D. *Angew. Chem., Int. Ed.* **2007**, *46*, 7548–7558. (b) Vivero-Escoto, J. L.; Slowing, I. I.; Trewyn, B. G.; Lin, V. S. Y. *Small* **2010**, *6*, 1952–1967. (c) Hoffmann, F.; Cornelius, M.; Morell, J.; Fröba, M. *Angew. Chem., Int. Ed.* **2006**, *45*, 3216–3251. (d) Li, Z.; Barnes, J. C.; Bosoy, A.; Stoddart, J. F.; Zink, J. I. *Chem. Soc. Rev.* **2012**, *41*, 2590–2605. (e) Soler-Illia, G. J. d. A.; Sanchez, C.; Lebeau, B.; Patarin, J. *Chem. Rev.* **2002**, *102*, 4093–4138.
- (2) (a) Hudson, S.; Cooney, J.; Magnier, E. *Angew. Chem., Int. Ed.* **2008**, *47*, 8582–8594. (b) Cipolatti, E. P.; Silva, M. J. A.; Klein, M.; Feddern, V.; Feltes, M. M. C.; Oliveira, J. V.; Ninow, J. L.; de Oliveira, D. *J. Mol. Catal. B: Enzym.* **2014**, *99*, 56–67. (c) Zucca, P.; Sanjust, E. *Molecules* **2014**, *19*, 14139–14194. (d) Hanefeld, U.; Gardossi, L.; Magnier, E. *Chem. Soc. Rev.* **2009**, *38*, 453–468.
- (3) (a) Stein, A.; Wang, Z.; Fierke, M. A. *Adv. Mater.* **2009**, *21*, 265–293. (b) Slowing, I. I.; Trewyn, B. G.; Giri, S.; Lin, V. S. Y. *Adv. Funct. Mater.* **2007**, *17*, 1225–1236. (c) Huh, S.; Wiench, J. W.; Yoo, J.-C.; Pruski, M.; Lin, V. S. Y. *Chem. Mater.* **2003**, *15*, 4247–4256.
- (4) Zhou, H. C.; Long, J. R.; Yaghi, O. M. *Chem. Rev.* **2012**, *112*, 673–674.
- (5) (a) Sumida, K.; Rogow, D. L.; Mason, J. A.; McDonald, T. M.; Bloch, E. D.; Herm, Z. R.; Bae, T.-H.; Long, J. R. *Chem. Rev.* **2012**, *112*, 724–781. (b) Yoon, M.; Srirambalaji, R.; Kim, K. *Chem. Rev.* **2012**, *112*, 1196–1231. (c) Li, J.-R.; Sculley, J.; Zhou, H.-C. *Chem. Rev.* **2012**, *112*, 869–932. (d) Wu, H.; Gong, Q.; Olson, D. H.; Li, J. *Chem. Rev.* **2012**, *112*, 836–868. (e) Zhang, T.; Lin, W. *Chem. Soc. Rev.* **2014**, *43*, 5982–5993.
- (6) (a) Song, L.; Zhang, J.; Sun, L.; Xu, F.; Li, F.; Zhang, H.; Si, X.; Jiao, C.; Li, Z.; Liu, S.; Liu, Y.; Zhou, H.; Sun, D.; Du, Y.; Cao, Z.; Gabelica, Z. *Energy Environ. Sci.* **2012**, *5*, 7508–7520. (b) Deng, H.; Grunder, S.; Cordova, K. E.; Valente, C.; Furukawa, H.; Hmadedh, M.; Gándara, F.; Whalley, A. C.; Liu, Z.; Asahina, S.; Kazumori, H.; O’Keeffe, M.; Terasaki, O.; Stoddart, J. F.; Yaghi, O. M. *Science* **2012**, *336*, 1018–1023. (c) Hwang, Y. K.; Hong, D. Y.; Chang, J. S.; Jhung, S. H.; Seo, Y. K.; Kim, J.; Vimont, A.; Daturi, M.; Serre, C.; Férey, G. *Angew. Chem., Int. Ed.* **2008**, *47*, 4144–4148. (d) Park, Y. K.; Choi, S. B.; Kim, H.; Kim, K.; Won, B.-H.; Choi, K.; Choi, J.-S.; Ahn, W.-S.; Won, N.; Kim, S.; Jung, D. H.; Choi, S.-H.; Kim, G.-H.; Cha, S.-S.; Jhon, Y. H.; Yang, J. K.; Kim, J. *Angew. Chem., Int. Ed.* **2007**, *46*, 8230–8233. (e) Koh, K.; Wong-Foy, A. G.; Matzger, A. J. *Angew. Chem., Int. Ed.* **2008**, *47*, 677–680. (f) Koh, K.; Wong-Foy, A. G.; Matzger, A. J. *J. Am. Chem. Soc.* **2009**, *131*, 4184–4185. (g) Férey, G.; Serre, C.; Mellot-Draznieks, C.; Millange, F.; Surblé, S.; Dutour, J.; Margiolaki, I. *Angew. Chem., Int. Ed.* **2004**, *43*, 6296–6301. (h) Furukawa, H.; Ko, N. Y.; Go, B.; Aratani, N.; Choi, S. B.; Choi, E. A.; Yazaydin, O.; Snurr, R. Q.; O’Keeffe, M.; Kim, J.; Yaghi, O. M. *Science* **2010**, *329*, 424–428. (i) Mondloch, J. E.; Bury, W.; Fairen-Jimenez, D.; Kwon, S.; DeMarco, E. J.; Weston, M. H.; Sarjeant, A. A.; Nguyen, S. T.; Stair, P. C.; Snurr, R. Q.; Farha, O. K.; Hupp, J. T. *J. Am. Chem. Soc.* **2013**, *135*, 10294–10297. (j) Yuan, D.; Zhao, D.; Sun, D.; Zhou, H.-C. *Angew. Chem., Int. Ed.* **2010**, *49*, 5357–5361. (k) Farha, O. K.; Eryazici, I.; Jeong, N. C.; Hauser, B. G.; Wilmer, C. E.; Sarjeant, A. A.; Snurr, R. Q.; Nguyen, S. T.; Yazaydin, A. Ö.; Hupp, J. T. *J. Am. Chem. Soc.* **2012**, *134*, 15016–15021. (l) Feng, D.; Gu, Z.-Y.; Li, J.-R.; Jiang, H.-L.; Wei, Z.; Zhou, H.-C. *Angew. Chem., Int. Ed.* **2012**, *51*, 10307–10310. (m) Morris, W.; Voloskiy, B.; Demir, S.; Gándara, F.; McGrier, P. L.; Furukawa, H.; Cascio, D.; Stoddart, J. F.; Yaghi, O. M. *Inorg. Chem.* **2012**, *51*, 6443–6445. (n) Horcajada, P.; Chevreau, H.; Heurtaux, D.; Benyettou, F.; Salles, F.; Devic, T.; Garcia-Marquez, A.; Yu, C.; Lavrard, H.; Dutson, C. L.; Magnier, E.; Maurin, G.; Elkaim, E.; Serre, C. *Chem. Commun.* **2014**, *50*, 6872–6874.
- (7) (a) Férey, G.; Mellot-Draznieks, C.; Serre, C.; Millange, F.; Dutour, J.; Surblé, S.; Margiolaki, I. *Science* **2005**, *309*, 2040–2042. (b) Chen, Y.; Lykourinou, V.; Vetromile, C.; Hoang, T.; Ming, L.-J.; Larsen, R. W.; Ma, S. *J. Am. Chem. Soc.* **2012**, *134*, 13188–13191.
- (8) (a) Senkovska, I.; Kaskel, S. *Chem. Commun.* **2014**, *50*, 7089–7098. (b) Wang, X.-S.; Ma, S.; Sun, D.; Parkin, S.; Zhou, H.-C. *J. Am. Chem. Soc.* **2006**, *128*, 16474–16475. (c) Zhuang, W. J.; Ma, S.; Wang, X.-S.; Yuan, D.; Li, J.-R.; Zhao, D.; Zhou, H.-C. *Chem. Commun.* **2010**, *46*, 5223–5225. (d) Liu, C.; Li, T.; Rosi, N. L. *J. Am. Chem. Soc.* **2012**, *134*, 18886–18888.
- (9) Feng, D.; Liu, T.-F.; Su, J.; Bosch, M.; Wei, Z.; Wan, W.; Chen, Y.-P.; Wang, X.; Wang, K.; Lian, X.; Gu, Z.-Y.; Park, J.; Yuan, D.; Zou, X.; Zhou, H.-C. *Nat. Commun.* **2014**, DOI: 10.1038/ncomms6979.
- (10) Feng, D.; Wang, K.; Wei, Z.; Chen, Y.-P.; Simon, C. M.; Arvapally, R. K.; Martin, R. L.; Bosch, M.; Liu, T.-F.; Fordham, S.; Yuan, D.; Omary, M. A.; Haranczyk, M.; Smit, B.; Zhou, H.-C. *Nat. Commun.* **2014**, *5*, No. 5723.
- (11) (a) Wang, Z.; Cohen, S. M. *Chem. Soc. Rev.* **2009**, *38*, 1315–1329. (b) Burnett, B. J.; Barron, P. M.; Hu, C.; Choe, W. *J. Am. Chem. Soc.* **2011**, *133*, 9984–9987. (c) Tanabe, K. K.; Cohen, S. M. *Chem. Soc. Rev.* **2011**, *40*, 498–519. (d) Karagiariidi, O.; Bury, W.; Sarjeant, A. A.; Stern, C. L.; Farha, O. K.; Hupp, J. T. *Chem. Sci.* **2012**, *3*, 3256–3260. (e) Karagiariidi, O.; Lalonde, M. B.; Bury, W.; Sarjeant, A. A.; Farha, O. K.; Hupp, J. T. *J. Am. Chem. Soc.* **2012**, *134*, 18790–18796. (f) Kim, M.; Cahill, J. F.; Fei, H. H.; Prather, K. A.; Cohen, S. M. *J. Am. Chem. Soc.* **2012**, *134*, 18082–18088. (g) Kim, M.; Cahill, J. F.; Su, Y. X.; Prather, K. A.; Cohen, S. M. *Chem. Sci.* **2012**, *3*, 126–130. (h) Bury, W.; Fairen-Jimenez, D.; Lalonde, M. B.; Snurr, R. Q.; Farha, O. K.; Hupp, J. T. *Chem. Mater.* **2013**, *25*, 739–744. (i) Fei, H.; Cahill, J. F.; Prather, K. A.; Cohen, S. M. *Inorg. Chem.* **2013**, *52*, 4011–4016. (j) Gross, A. F.; Sherman, E.; Mahoney, S. L.; Vajo, J. J. *J. Phys. Chem. A* **2013**, *117*, 3771–3776. (k) Hirai, K.; Chen, K.; Fukushima, T.; Horike, S.; Kondo, M.; Louvain, N.; Kim, C.; Sakata, Y.; Meilikhov, M.; Sakata, O.; Kitagawa, S.; Furukawa, S. *Dalton Trans.* **2013**, *42*, 15868–15872. (l) Jeong, S.; Kim, D.; Song, X.; Choi, M.; Park, N.; Lah, M. S. *Chem. Mater.* **2013**, *25*, 1047–1054. (m) Karagiariidi, O.; Bury, W.; Tylianakis, E.; Sarjeant, A. A.; Hupp, J. T.; Farha, O. K. *Chem. Mater.* **2013**, *25*, 3499–3503. (n) Kim, S.; Dawson, K. W.; Gelfand, B. S.; Taylor, J. M.; Shimizu, G. K. H. *J. Am. Chem. Soc.* **2013**, *135*, 963–966. (o) Li, T.; Kozlowski, M. T.; Doud, E. A.; Blakely, M. N.; Rosi, N. L. *J. Am. Chem. Soc.* **2013**, *135*, 11688–11691. (p) Takaishi, S.; DeMarco, E. J.; Pellin, M. J.; Farha, O. K.; Hupp, J. T. *Chem. Sci.* **2013**, *4*, 1509–1513. (q) Valtchev, V.; Majano, G.; Mintova, S.; Perez-Ramirez, J. *Chem. Soc. Rev.* **2013**, *42*, 263–290. (r) Deria, P.; Mondloch, J. E.; Karagiariidi, O.; Bury, W.; Hupp, J. T.; Farha, O. K. *Chem. Soc. Rev.* **2014**, *43*, 5896–5912. (s) Han, Y.; Li, J.-R.; Xie, Y.; Guo, G. *Chem. Soc. Rev.* **2014**, *43*, 5952–5981. (t) Hong, D. H.; Suh, M. P. *Chem.—Eur. J.* **2014**, *20*, 426–434. (u) Jeong, S.; Kim, D.; Shin, S.; Moon, D.; Cho, S. J.; Lah, M. S. *Chem. Mater.* **2014**, *26*, 1711–1719. (v) Karagiariidi, O.; Bury, W.; Mondloch, J. E.; Hupp, J. T.; Farha, O. K. *Angew. Chem., Int. Ed.* **2014**, *53*, 4530–4540. (w) Morabito, J. V.; Chou, L.-Y.; Li, Z.; Manna, C. M.; Petroff, C. A.; Kyada, R. J.; Palomba, J. M.; Byers, J. A.; Tsung, C.-K. *J. Am. Chem. Soc.* **2014**, *136*, 12540–12543. (x) Szilagyi, P. A.; Weinrauch, I.; Oh, H.; Hirscher, M.; Juan-Alcaniz, J.; Serra-Crespo, P.; de Respinis, M.; Trzesniewski, B. J.; Kapteijn, F.; Geerlings, H.; Gascon, J.; Dam, B.; Grzech, A.; van de Krol, R.; Geerlings, H. *J. Phys. Chem. C* **2014**, *118*, 19572–19579. (y) Brozek, C. K.; Dincă, M. *Chem. Soc. Rev.* **2014**, *43*, 5456–5467. (z) Liu, T. - F.; Zou, L.; Feng, D.; Chen, Y.-P.; Fordham, S.;

Wang, X.; Liu, Y.; Zhou, H.-C. *J. Am. Chem. Soc.* **2014**, *136*, 7813–7816.

(13) Savonnet, M.; Bazer-Bachi, D.; Bats, N.; Perez-Pellitero, J.; Jeanneau, E.; Lecocq, V.; Pinel, C.; Farrusseng, D. *J. Am. Chem. Soc.* **2010**, *132*, 4518–4519.

(14) (a) Tanabe, K. K.; Cohen, S. M. *Chem. Soc. Rev.* **2011**, *40*, 498–519. (b) Yu, C.-J.; Wu, S.-M.; Tseng, W.-L. *Anal. Chem.* **2013**, *85*, 8559–8565. (c) Taylor-Pashow, K. M. L.; Rocca, J. D.; Xie, Z.; Tran, S.; Lin, W. *J. Am. Chem. Soc.* **2009**, *131*, 14261–14263.